Structural Study of $LiCoO_2$ Synthesized by Sol-Gel Method at Different Temperatures

Monika[a], Anjali, Ashish Kumar Mishra, Raj Kumar Jagota and Balbir Singh Patial[b]

Department of Physics, Himachal Pradesh University Summerhill, Shimla, Himachal Pradesh-171005, India.

[a] monika2019panghal@gmail.com
[b] bspatial@hpuniv.ac.in

Abstract

Minimizing environmental impact requires efficient energy storage, which is essential for the transition to renewable energy. Lithium-ion batteries (LIBs) are widely recognized for offering high energy density and long lifespan, making them a key technology in this transition. Their lightweight design also helps lower emissions in portable devices, contributing to a more sustainable energy future. A critical component of LIB is the cathode material, which plays a vital role in determining the battery's overall performance, capacity, and stability. Among the various cathode materials, $LiCoO_2$ is widely used due to its excellent electrochemical properties and stability. In order to find out how temperature affects the structural and morphological characteristics of $LiCoO_2$, it was synthesized using the sol-gel process conducted at various temperatures. Utilizing X-ray diffraction (XRD), the study confirmed the crystallinity and defects while field emission scanning electron microscopy (FESEM) was employed to study the surface structure and to determine particle size. The impact of temperature on the structural characteristics of $LiCoO_2$ is reported and discussed in detail.

Keywords: Cathode Material, $LiCoO_2$, Sol-gel Method, FESEM, XRD.
Received 30 January 2025; First Review 21 February 2025; Accepted 13 April 2025.

*** Address of correspondence**
Balbir Singh Patial
Department of Physics, Himachal Pradesh University Summerhill, Shimla, Himachal Pradesh-171005, India.

Email: bspatial@gmail.com

How to cite this article
Monika, Anjali, Ashish Kumar Mishra, Raj Kumar Jagota and Balbir Singh Patial, Structural Study of $LiCoO_2$ Synthesized by Sol-Gel Method at Different Temperatures, J. Cond. Matt. 2025; 03 (02): 114-117.

Available from:
https://doi.org/10.61343/jcm.v3i02.118

Introduction

The development of high-energy density batteries has become a top priority due to ever increasing demand for energy storage. The depletion of non-renewable resources like coal and petroleum along with their environmental impact, serves as a strong push toward a transition to renewable energy sources. Renewable energy sources that are naturally available such as solar, wind, biomass, tidal, and geothermal energy, are safe for the environment and do not contribute to global warming by emitting harmful greenhouse gases.

$LiCoO_2$ is one of the widely used cathode materials due to its better electrochemical properties and high stability. The crystal structure, particle size, and overall distribution of $LiCoO_2$ are greatly influenced by the choice of material and synthesis method. Among the various techniques, the sol-gel method offers significant advantages due to its capability to control factors like surface area, particle size, and morphology, key element for improving Li-ion diffusion and enhancing electrode performance. In this process, precursor solution underwent hydrolysis to form colloidal sol or gel, when the gel is further heated, it transforms into the desired material with enhanced properties. In order to maintain stoichiometry control and produce small, evenly distributed particles, chelating agents are used.

In this study, $LiCoO_2$ was synthesized using the sol-gel method to explore how different temperatures affect its morphology and structure. X-ray diffraction (XRD) was used to analyse the nature, crystallinity and defects, while FESEM was employed to study the surface structure and to deduce particle size. The influence of temperature on $LiCoO_2$'s structural characteristics is investigated to contribute to the development of high-performance cathode materials for LIBs [1-4].

Experimental details

Material Synthesis

To prepare $LiCoO_2$, a solution was created with $LiNO_3$ and Co $(NO_3)_2 \cdot 6H_2O$ in distilled water, maintaining Li: Co ratio as 1.1:1 as outlined by Predoana et al. [5]. A complexing agent, citric acid, was dissolved in water and

added to the solution. The mixture was heated to 70–80 °C under continuous magnetic stirring until it formed a gel. After the formation of the gel, one sample $LiCoO_2$ referred as LC80, was maintained at 80 °C until it converted to ash as the final product. Another similar composition sample, $LiCoO_2$ referred as LC300 was heated in the 250–300 °C range until it also transformed into ash completing to the final product. Thereafter, both the samples were placed at room temperature to cool down at its own. The crystalline powders were obtained using a two-step process in a muffle furnace. The first step involved calcination of the materials at 300 °C for 20 to 30 minutes, followed by a second stage of sintering at 700 °C for 24 hours.

X-ray diffraction (XRD) Study

It is one of the essential techniques in materials science, is used to analyze precise information and to examine the atomic-level crystallographic structure of both natural and synthetic materials. Because of the rotational projection of the randomly oriented reciprocal lattices, the powder diffraction pattern yields one-dimensional data instead of the three-dimensional position of each reflection. A prism or grating can be used to separate light into distinct frequencies, similar to the mechanism of an infrared prism. Every crystalline material has a unique diffraction pattern, and each phase in a mixture of crystalline substances generates a distinct pattern. This pattern is like a fingerprint, making it suitable for the characterization of polycrystalline phases.

The analysis of diffraction is governed by Bragg's law. The peaks that are seen when X-rays are diffracted from a crystal's lattice planes are indication of constructive interference.

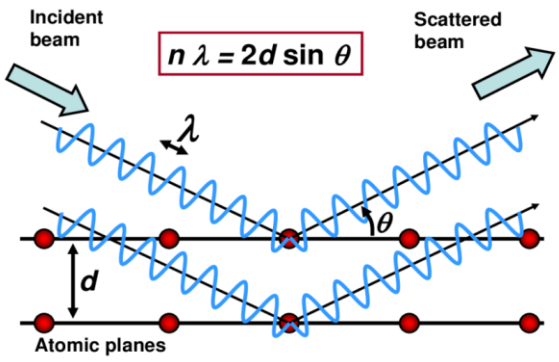

Figure 1: X-ray diffraction.

The inter-planar distance is represented by *d*, X-ray wavelength by "λ", and the incident angle by "θ" in this case, where n represents the order of constructive interference.

XRD measurements were performed across a 2θ range from $0° < 2\theta < 90°$ to examine the structural properties of the samples (LC80 and LC300). Crystalline size (D), dislocation density and microstrain (ε), were determined. The Crystalline size was determined using the Scherrer equation [6]:

$$D = K\lambda / \beta \cos\theta \quad (1)$$

where (K) is the shape factor (here 0.9), (λ) is the wavelength of the X-ray source which is 0.154 nm, (β) is the full width at half maximum (FWHM) in radians, and (θ) is the Bragg angle (half of the 2θ angle), also converted into radians for accurate calculations.

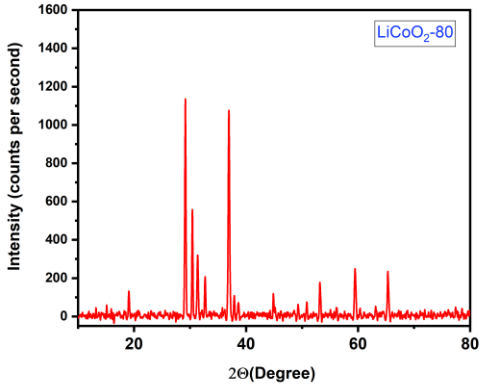

Figure 2: XRD of LC80.

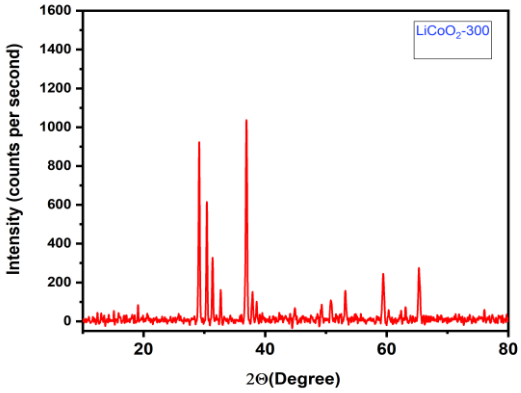

Figure 3: XRD of LC300.

XRD pattern of LC300 displaying a decrease in peak intensity as compared to LC80, suggesting decreasing intensity with the increase in temperature.

Material characterization using FESEM

The incident electrons will exhibit a hemispheric diffusion if the specimen's element has a high atomic number, and a teardrop-shaped diffusion if the element has a low atomic number. The diffusion area can be expanded significantly deeper with higher accelerating voltages. The incident electrons may progressively lose energy during diffusion until they are absorbed by the specimen (shown as absorbed current). Low energy secondary electrons lose a significant

amount of energy during this process and are reflected outside the specimen. When incident electrons interact with the constituent atoms of a specimen, most of the electron energy is converted into heat, while some of it is used to generate secondary electrons, Auger electrons, X-rays, and visible or infrared cathodoluminescence. Auger electrons, in particular, are emitted from regions very close to the specimen's surface.

Information describing the specimen's nature is conveyed through X-rays, backscattered electrons, quanta (secondary electrons), and other sources. FESEM makes it possible to observe the material's porosity, surface characteristics, structure, particle size and shape. A beam of electrons is focused on the sample's surface after being accelerated across a potential difference. An electron beam is typically generated using sources such as a tungsten filament cathode, a lanthanum (LaB_6) wire, or an electron gun. In the case of an electron gun, an emitter is maintained at a negative potential relative to a nearby electrode and the resulting potential difference at the emitter surface enables field electron emission.

The analyzer detects the electromagnetic radiation emitted from the sample. In FESEM, image formation is mainly due to secondary electrons, which are the most abundant among the emitted electrons. A current is created and recorded once the secondary electrons arrive at the detector. An image is created by charting the current on the sample's surface against the probe position. Since surface morphology plays a key role in contrast, the final image directly represents the surface structure [7].

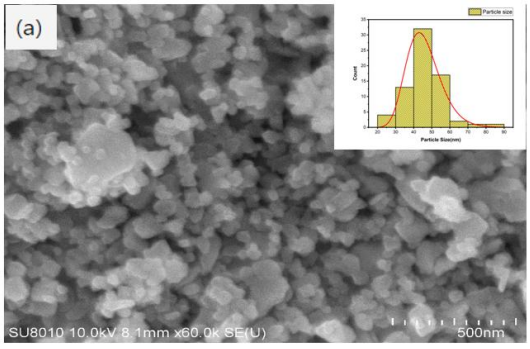

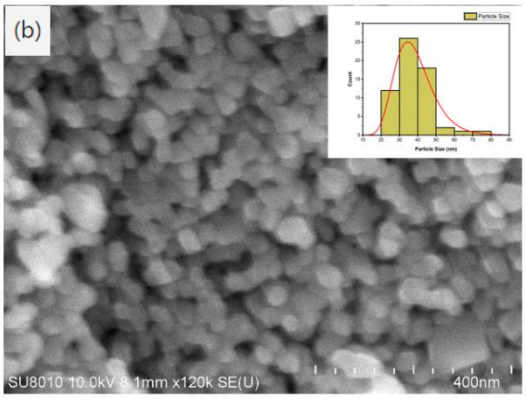

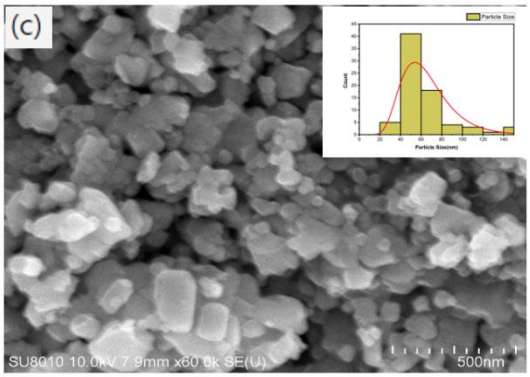

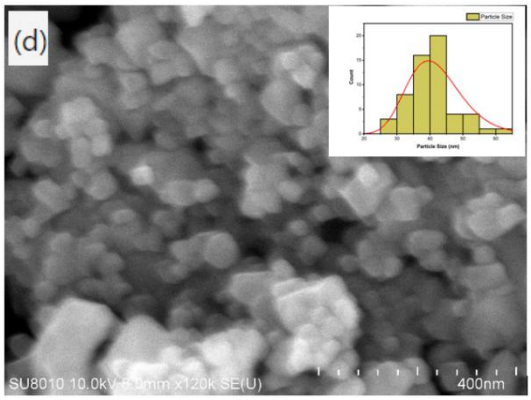

Figure 4: FESEM micrographs **(a) ×60k** (LC80), **(b) ×120k** (LC80), **(c) ×60k** (LC300), **(d) ×120k** (LC300) (inset for all figures shows nanocrystalline particle size distribution).

Results and discussion

The quantity of defects and imperfections within a crystal lattice is represented by the system's dislocation density, calculated using the following relation [8]:

$$\delta = 1/D^2 \qquad (2)$$

Additionally, the microstrain (ε) arises due to the displacement of atoms relative to their ideal lattice positions. It can be determined using the expression:

$$\varepsilon = \beta \cos \theta /4 \qquad (3)$$

For LC80, the crystalline size ranges from a minimum of 32.38 nm (at $2\theta = 36.94°$) to a maximum of 54.10 nm (at $2\theta = 30.41°$). The dislocation density for LC80 varies between 0.342×10^{-3} and 0.954×10^{-3}, and the microstrain ranges from 0.64×10^{-3} to 1.07×10^{-3}. In comparison, LC300 has a crystalline size range from 29.49 nm (at $2\theta = 65.33°$) to 46.67 nm (at $2\theta = 30.41°$), a dislocation density between 0.459×10^{-3} and 1.150×10^{-3}, and a microstrain range of 0.74×10^{-3} to 1.18×10^{-3}. These variations in crystalline size, dislocation density, and microstrain reflect different levels of crystallinity, defect concentration, and lattice distortion, which may influence each sample's performance and stability in applications. Table 1, Table 2 summarizes the XRD data of paper and highlights notable differences

between LC80 and LC300 in terms of crystallinity and structural properties. The variations in crystalline size and dislocation density across 2θ values indicate different degrees of lattice integrity and imperfections in the samples.

Table 1: Crystalline Size, Dislocation Density, Microstrain of LC80.

Sample	2θ	FWHM	Crystalline Size (nm)	Dislocation Density ($\times10^{-3}$) (nm^{-2})	Microstrain ($\varepsilon \times10^{-3}$)
LC80	29.16	0.19	41.17	0.59	0.84
	30.41	0.15	54.10	0.34	0.64
	31.36	0.22	36.53	0.74	0.95
	36.94	0.25	32.38	0.95	1.07
	53.20	0.20	42.71	0.54	0.81
	59.48	0.26	34.25	0.85	1.01
	65.34	0.23	39.85	0.63	0.87

Table 2: Crystalline Size, Dislocation Density, Microstrain of LC300.

Sample	2θ	FWHM	Crystalline Size (nm)	Dislocation Density ($\times10^{-3}$) (nm^{-2})	Microstrain ($\varepsilon \times10^{-3}$)
LC 300	29.15	0.21	38.25	0.68	0.91
	30.41	0.17	46.67	0.45	0.74
	31.35	0.18	44.42	0.50	0.78
	36.92	0.25	32.57	0.94	1.06
	53.20	0.22	40.12	0.62	0.86
	59.43	0.30	29.56	1.14	1.17
	65.33	0.31	29.49	1.15	1.18

From XRD, Figures 2 and 3, it is clear that there is a decrease in peak intensity with increasing temperature, suggesting a higher degree of structural disorder. This may introduce more defect sites that act as charge-trapping centres and reduces overall charge storage efficiency. Additionally, the higher synthesis temperature results in more pronounced particle agglomeration, as evidenced by FESEM analysis. This agglomeration can reduce the effective surface area available for lithium-ion diffusion, potentially limiting electrochemical reaction kinetics.

Conclusions

As the temperature increases, corresponding rise in agglomeration is observed, which is evident from the FESEM analysis. The distinction between particle size and crystalline size becomes more pronounced at higher temperatures. In contrast, at lower temperature, there is minimal variation between the particle size and crystalline size. XRD analysis further reveals a decrease in the intensity of XRD peaks with increasing temperature, highlighting structural changes occurring during the process. Defects such as dislocation density and microstrain, which refer to distortions and strain within the crystal lattice, also increase with temperature, further affecting the material's properties.

Acknowledgement

We, first author (Monika), coauthor (Raj Kumar Jagota, Co-PI) and corresponding author (Balbir Singh Patial, Principal Investigator) extend our heartfelt gratitude to the Himachal Pradesh Council for Science, Technology and Environment (HIMCOSTE), Shimla HP (INDIA), for the financial assistance in supporting the research project (Registration No. HIMCOSTE(R&D)/2023 24-7(2)).

References

1. P Ghosh, S Mahanty, M W Raja, R N Basu, and H S Maiti. Journal of Materials Research 22: 1162–1167, 2007.
2. J Graetz, A Hightower, C C Ahn, R Yazami, P Rez, and B Fultz. Journal of Physical Chemistry B 106: 1286–1289, 2002.
3. Monika, A K Mishra, and B S Patial. Sustainable Chemistry One World 5: 100042, 2024.
4. A K Mishra, Monika, and B S Patial. Materials Today Electronics 7: 100089, 2024.
5. L Predoana, A Jitianu, M Voicescu, N G Apostol, and M Zaharescu. Journal of Sol-Gel Science and Technology 74: 406, 2015.
6. A L Patterson. Physical Review 56: 978, 1939
7. S Nallusamy, and A M Babu. Journal of Nano Research 37: 58–67, 2016.
8. Monika, A K Mishra, and B S Patial. Journal of Condensed Matter 1: 65–68, 2023.